IEEE Access
Multidisciplinary | Rapid Review | Open Access Journal

SPECIAL SECTION ON DATA ANALYTICS AND ARTIFICIAL INTELLIGENCE FOR PROGNOSTICS AND HEALTH MANAGEMENT (PHM) USING DISPARATE DATA STREAMS

Received January 2, 2020, accepted January 13, 2020, date of publication January 23, 2020, date of current version January 31, 2020.

Digital Object Identifier 10.1109/ACCESS.2020.2968939

LSTM-Based Battery Remaining Useful Life Prediction With Multi-Channel Charging Profiles

KYUNGNAM PARK[1], YOHWAN CHOI[1], WON JAE CHOI[2], HEE-YEON RYU[2], AND HONGSEOK KIM[1], (Senior Member, IEEE)

[1]Department of Electronic Engineering, Sogang University, Seoul 04107, South Korea
[2]Hyundai Motors, Inc., Seoul 16082, South Korea

Corresponding author: Hongseok Kim (hongseok@sogang.ac.kr)

This work was supported by the Basic Science Research Program through the National Research Foundation of Korea (NRF) funded by the Ministry of Science and ICT under Grant NRF-2017R1A1A1A05001377, and by the Hyundai Motors.

ABSTRACT Remaining useful life (RUL) prediction of lithium-ion batteries can reduce the risk of battery failure by predicting the end of life. In this paper, we propose novel RUL prediction techniques based on long short-term memory (LSTM). To estimate RUL even in the presence of capacity regeneration phenomenon, we consider multiple measurable data from battery management system such as voltage, current and temperature charging profiles whose patterns vary as aging. Unlike the traditional LSTM prediction that matches input layer with output layer as one-to-one structure, we leverage many-to-one structure to be flexible for various input types and to substantially reduce the number of parameters for better generalization. Using the NASA lithium-ion battery datasets, we verify the accuracy of the proposed LSTM-based RUL prediction. The experimental results show that the proposed single-channel LSTM model improves the mean absolute percentage error (MAPE) by 39.2% compared to the baseline LSTM model. Furthermore, the proposed multi-channel LSTM model significantly improves the MAPE, e.g., by 63.7% compared to the baseline; the proposed model achieves 0.47–1.88% of MAPE while the state-of-the-art baseline LSTM shows 0.6–6.45% of MAPE.

INDEX TERMS Lithium-ion battery, long short-term memory, remaining useful life, capacity estimation.

I. INTRODUCTION

Lithium-ion batteries are now widely used for many applications such as home appliances, smartphones, power tools, energy storage systems and electric vehicles because of high energy density, high electromotive force, high output voltage, low self-discharge, low voltage drop and easy management [1], [2]. However, battery degradation begins immediately after batteries are manufactured, and when 70% or 80% of initial capacity remains, batteries need be replaced for safe operation [3]. Thus, it is important to predict when battery life will be over [4].

Prognostics and health management (PHM) technology collects status information from machines, facilities, aviation, and power plants to detect abnormalities of the system and to optimize facility management by proactively predicting the point of failure through analysis and predictive verification [1]. The PHM in the battery can be seen as predicting the remaining useful life (RUL) to prevent losses from unexpected failures in advance [5], [6].

Batteries are not linearly degraded but are subject to degradation with irregular regeneration. Therefore, in order to accurately predict the RUL of battery, battery characteristics other than the current capacity need to be considered. In addition, the battery produces electricity through electrochemical reaction, and the total available capacity decreases as the battery is repeatedly charged and discharged. That is, the active material that affects the output power and the available capacity of battery are reduced due to repeated chemical reactions, and this results in performance degradation. Therefore, it is important to exploit diverse data related to battery life for accurate RUL prediction [7].

Battery RUL prediction approaches can be categorized into three cases: experience-based methods, model-based

The associate editor coordinating the review of this manuscript and approving it for publication was Faisal Khan.

methods and data-driven methods. Experience-based methods predict RUL using the stochastic deterioration distribution that does not require complex theories but have the drawback of non-real-time monitoring [8]. Model-based methods update the physical model in real-time from monitored data of usage conditions/defects to predict RUL [9]. While accurate RUL prediction is possible without using a large volume of data, there are not well-established failure physical models. Finally, data-driven methods obtain the relationship using machine learning techniques from the monitored data of usage conditions/defects and extrapolate it into future conditions.

Specifically, data-driven methods rely solely on historical capacity degradation data rather than requiring explicit mathematical models of battery degradation or internal mechanisms of the battery [10]–[12]. For example, Nuhic et al. used support vector machine (SVM) to predict lithium-ion battery's state of health (SoH) and RUL [10], and Liu et al. proposed the relevance vector machine (RVM) algorithm, an online training method, to improve the accuracy of RUL prediction [11]. Patil et al. have devised an online multi-stage SVM method utilizing battery voltage and temperature data as characteristic parameters to improve the accuracy of RUL prediction [12]. However, these algorithms require a large amount of historical data to learn the patterns of battery capacity degradation, and in case battery degradation data are highly nonlinear, forecasting accuracy may not be guaranteed.

To overcome these limitations, neural network techniques are employed to predict the lithium-ion battery RUL [13]–[15]. Liu et al. introduced the adaptive recurrent neural network (RNN) for predicting RUL by estimating the dynamic state of battery [13]. Using NASA's battery data on lithium-ion degradation, the authors verified that RNN is better than RVM and particle filter techniques. However, RNN has the long-term dependency problem [16] as the number of cycles (i.e., charging and discharging) increases. Very recently, Zhang *et al.* [14] used long short-term memory (LSTM) to reflect long-term memories of battery degradation tendency. In addition, combining LSTM and other model is proposed for RUL prediction [15]. However, these LSTM predictions did not capture the *capacity regeneration*, the irregular capacity increase, which cannot be well predicted by using capacity data only. In addition, LSTM basically requires a large number of parameters for training. To overcome the shortcoming of LSTM with a large number of training parameters, Xiao *et al.* [17] used gated recurrent unit (GRU) to estimate the state of charge, and Song *et al.* [18] used GRU to predict the battery RUL. Song et al. found that GRU outperforms RVM, but they do not consider using various data as an efficient model structure.

In order to significantly improve the prediction accuracy even in the presence of capacity regeneration, we propose two learning methods using LSTM. We leverage the multi-channel measurable data of voltage, current and temperature charging profiles from battery management system (BMS) whose patterns vary with cycles as aging. In order to use this various data efficiently, unlike the traditional LSTM prediction that matches input layer with output layer as one-to-one structure (the same size of capacity vectors for input and output) [19], [20], we match input layer with output layer as many-to-one structure. The proposed LSTM-based RUL prediction method is partially related to our previous work [7]. However, [7] was focused on capacity estimation at the current cycle, but not on prediction. To verify the proposed techniques, we use the NASA battery datasets that exhibit diverse degradation patterns with different number of cycles.

We summarize our key contributions as follows. First, unlike previous methods using single-channel data only, i.e., capacity per cycle, we show that leveraging multi-channel charging profiles of voltage, current, and temperature significantly improves the RUL prediction accuracy even in the presence of capacity regeneration. Second, we propose to use the many-to-one structure to accommodate the multi-channel input for LSTM-based RUL prediction. This structure change reduces the number of parameters drastically, which is beneficial for generalization as well. On average, the number of parameters of the baseline LSTM is 22,295, while the number of parameters of the proposed LSTM is 725 in the case of single-channel and 2,772 in the case of multi-channel, which is an order of magnitude improvement. Third, our experiments show that the proposed methods significantly improve the RUL prediction accuracy. In the case of using single-channel data (capacity), the proposed method achieves 1.71% of mean absolute percentage error (MAPE) while the baseline shows 2.81% of MAPE. In the case of using multi-channel charging profiles, the proposed method achieves 1.02% of MAPE, which is 63.7% improvement over the baseline. Furthermore, the proposed technique outperforms other deep learning-based methods such as RNN, GRU and simple recurrent unit (SRU) [21] by 44.6%, 32.5% and 52.1%, respectively.

The rest of this paper is organized as follows. Section II describes battery capacity degradation and its relationship with charging profiles of voltage, current, and temperature. Section III describes traditional RUL prediction and the proposed multi-channel LSTM method. We present learning process and model selection in Section IV and the experimental results in Section V, followed by the conclusion in Section VI.

II. BATTERY DATA

A. BATTERY CAPACITY DEGRADATION

We use the battery datasets of NASA Prognostics Center of Excellence Data Repository, which consists of three different operating profiles of charging, discharging and impedance at room temperature [22]. Battery charging is performed by the constant-current constant-voltage (CCCV) principle; charging is done with the constant current of 1.5A until the voltage reaches the limit of 4.2V, then the voltage remains constant until the current drops to 20mA. For batteries #5, #6, #7, and #18 (following the numbering of the NASA datasets),

TABLE 1. Specification of batteries of NASA Prognostics center of excellence data repository.

Battery no.	Charging			Discharging		Operating conditions		
	Constant current (A)	Upper voltage limit (V)	Cut-off current (mA)	Constant current (A)	Cut-off voltage (V)	Operating temperature	Initial capacity (Ah)	Capacity retention
Battery #5	1.5	4.2	20	2	2.7	Room temp.	1.86	70.5%
Battery #6	1.5	4.2	20	2	2.5	Room temp.	2.04	57.7%
Battery #7	1.5	4.2	20	2	2.2	Room temp.	1.89	75.2%
Battery #18	1.5	4.2	20	2	2.5	Room temp.	1.86	73.0%

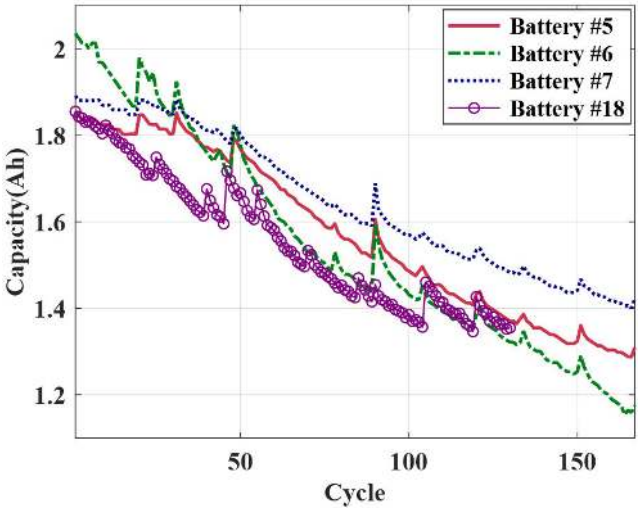

FIGURE 1. Capacity degradation over charging/discharging cycle.

discharging is done at constant current of 2A until the cell voltage drops to 2.7V, 2.5V, 2.2V and 2.5V, respectively. Table 1 summarizes the charging and discharging operation.

To quantify battery degradation, state of health (SoH) is by defined using capacity as follows [23]:

$$SoH\ (\%) = \frac{C_k}{C_0} \times 100 \tag{1}$$

where C_0 is the initial capacity and C_k is the measured capacity at cycle k. Starting from the different initial capacities, the batteries continuously degrade over time, and the final capacity of batteries #5, #6, #7, #18 are 70.5%, 57.7%, 75.2%, and 73.0%, respectively as shown in Table 1. The end of battery life is defined when the remaining capacity is 70 to 80% of the initial capacity, depending on applications. To fully utilize all four battery datasets, we set the end of life as the maximum retention at the last cycle. Fig. 1 shows the capacity degradation over cycle. Note that battery #5, #6, #7 has data measured up to 167 cycles while battery #18 has data measured up to 130 cycles only.

B. DATA ACQUISITION FROM CHARGING PROCESS

During charging, lithium-ions escape from the electrode particles, and conversely, lithium-ions enter the electrode particles during discharging. Lithium-ions are scattered irregularly across the surface of battery particles. The larger the irregularity, the more the battery particles are affected, and battery life becomes shorter. Thus, to predict the RUL of battery, we identify the characteristics of charging or discharging process using data. During discharging process, it is difficult to accurately measure or calculate the internal parameters because current varies rapidly over time. In addition, discharging pattern contains high randomness depending on the battery owner's usage pattern. By contrast, charging process is usually based on preset protocols, and the external electrical performance can be easily measured. Hence, in order to capture how internal battery parameters change along with aging, we leverage data from charging cycle.

C. MULTI-CHANNEL CHARGING PROFILES OF VOLTAGE, CURRENT, AND TEMPERATURE

Fig. 2 shows the charging profiles of voltage, current and temperature for different remaining capacities (i.e., SoH of 100%, 90%, 80% and 70%). As can be seen, the voltage of the aged battery reaches 4.2V earlier than the fresh one, and the current of the aged battery begins to drop from the constant current earlier than the fresh one. In addition, the aged batteries reach the maximum temperature faster than the fresh battery. This shows that the charging profiles of voltage, current, and temperature depend on SoH, and we leverage these *multi-channel charging features* to predict the remaining battery capacity in addition to historic capacity data $\{C_k\}$.

D. CAPACITY REGENERATION

Lithium-ions collected in the negative electrode move to the positive electrode during discharging, and electricity is generated. On the contrary, lithium-ions move from the positive electrode to the negative electrode during charging. As the lithium-ions move, unnecessary movement of negative-ions can cause unwanted secondary reactions on the electrode surface, resulting in poor battery performance, and degradation occurs. Interestingly, however, there is a re-balancing phenomenon of active materials and relaxation of gradients produced due to the current flow in the rest time, which increases the usable capacity of the next cycle [24]. This phenomenon is called capacity regeneration. Capacity regeneration alters the tendency of capacity degradation curve and affects the performance of the RUL prediction model. Hence, it is crucial to consider the capacity regeneration phenomenon in battery RUL prediction.

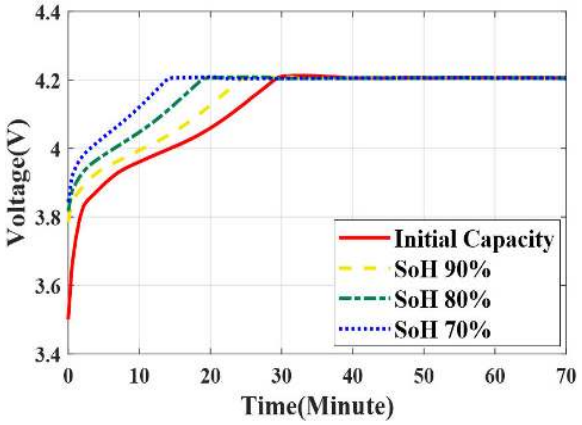

(a) Voltage

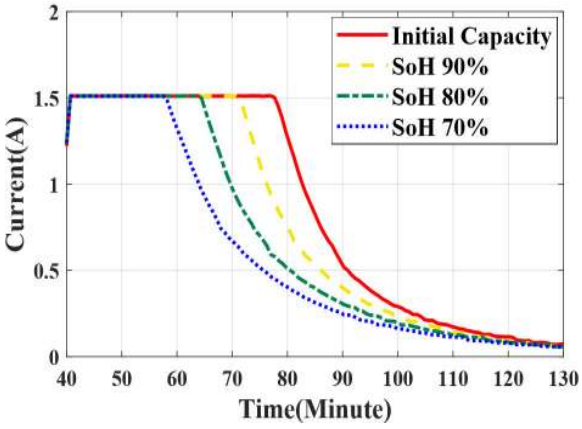

(b) Current

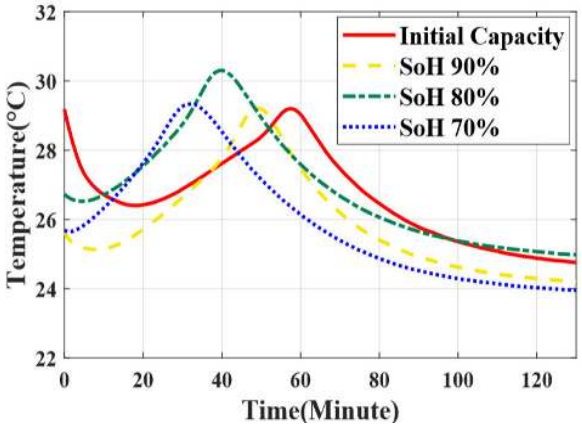

(c) Temperature

FIGURE 2. Battery charging profiles for various state of health.

III. METHODOLOGIES

A. LONG SHORT-TERM MEMORY

LSTM has been widely used for RUL prediction because LSTM is good for time series prediction [1], [15], [19], [20]. The basic structure of LSTM is as follows. Let x_k denote the input at the current time step k and h_{k-1} denote the output of the hidden layer at the previous time step $k-1$. The LSTM network architecture is shown in Fig. 3. The core of LSTM is the cell state c_k, which corresponds to the upper horizontal line in Fig. 3. The cell state allows the gradient to be well propagated even though the state has elapsed for quite a long time, and thus LSTM alleviates the vanishing gradient problem of the basic RNN.

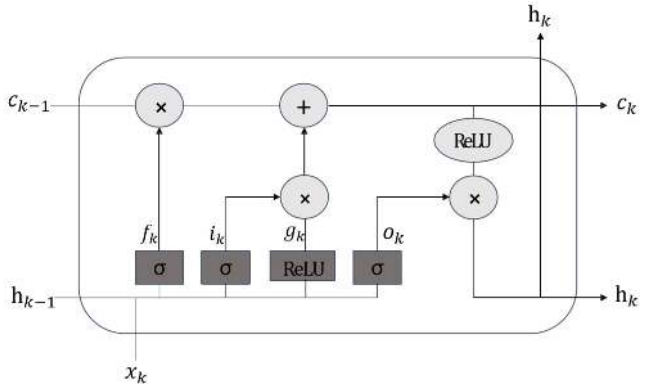

FIGURE 3. The cell structure of LSTM.

The first unit of LSTM is the forget gate f_k, and the input gate specifies the information to update. The new candidate value g_k is temporarily saved before a new cell state value is updated. At each stage, h_{k-1} and x_k are received as input, and the output is calculated with the parameters of weights and biases, and the sigmoid or rectified linear unit (ReLU) activation function. We use ReLU activation function to overcome the vanishing gradient problem. The gates are calculated as follows:

$$f_k = \sigma(W_x^f x_k + W_h^f h_{k-1} + b^f). \tag{2}$$

$$i_k = \sigma(W_x^i x_k + W_h^i h_{k-1} + b^i), \tag{3}$$

$$g_k = ReLU(W_x^g x_k + W_h^g h_{k-1} + b^g). \tag{4}$$

Then, the forget gate f_k is mixed by elementwise product with the cell state at the previous time step c_{k-1}, and the input gate i_k is mixed by elementwise product with new candidate value g_k. The sum of these two determines the cell state c_k,

$$c_k = f_k \odot c_{k-1} + i_k \odot g_k. \tag{5}$$

The last unit is the output gate o_k. This gate determines the information to output. Similar to the previous steps, the output gate is calculated as follows:

$$o_k = \sigma(W_x^o x_k + W_h^o h_{k-1} + b^o). \tag{6}$$

Finally, the hidden state h_t is computed by

$$h_k = o_k \odot ReLU(c_k). \tag{7}$$

In using LSTM for RUL prediction, the state-of-the-art technique uses only the historic capacity data $\{C_k\}$ as input [1], [15], and the input and output sizes are same [19], [20]. However, the same size of input and output implies that the *data type* of input and output should be identical. Thus, the traditional input and output formats of LSTM-based

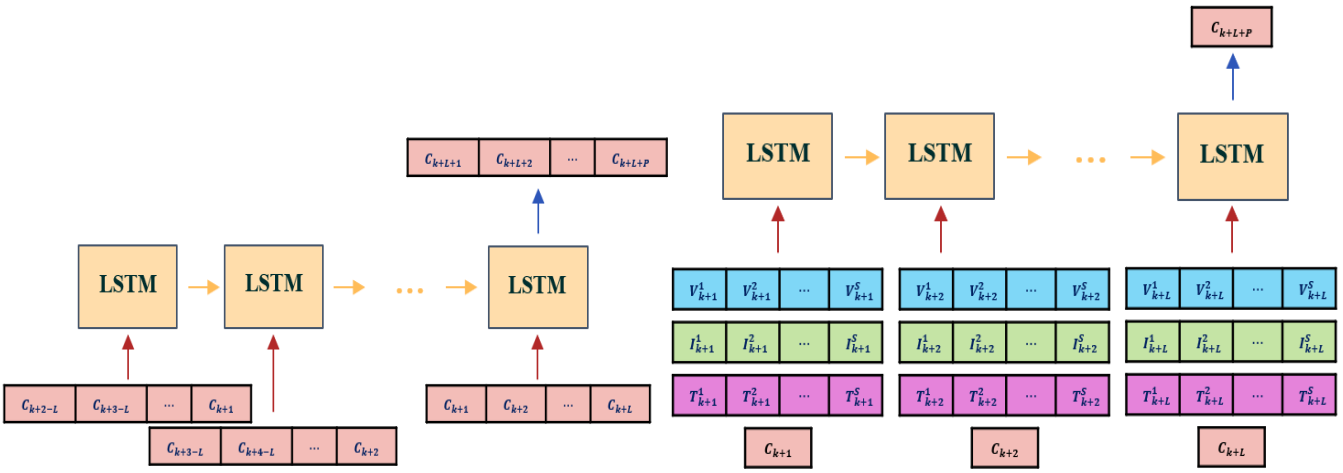

(a) One-to-one structure (b) Many-to-one structure

FIGURE 4. Input/output format of LSTM-base RUL prediction.

RUL prediction is given by

$$\begin{cases} (C_{k+2-L}, \ldots, C_{k+1}) \\ (C_{k+3-L}, \ldots, C_{k+2}) \\ \ldots \\ (C_{k+1}, \ldots, C_{k+L}) \end{cases} \rightarrow (C_{k+L+1}, \ldots, C_{k+L+P}) \quad (8)$$

where L is the input size, and P is the prediction interval. In this one-to-one structure, the length of the input is the same as that of the output, i.e., $L = P$. The LSTM of using (8) [19], [20] serves our baseline hereafter, and its structure is shown in Fig. 4(a).

B. PROPOSED LSTM MODEL FOR RUL PREDICTION

In one-to-one structure, training is based on a single type of time series data. However, it may not be efficient for RUL prediction when training data are limited. Furthermore, additional data such as voltage, current, and temperature cannot be used for input, either. Thus, we propose to use another structure, as shown in Fig. 4(b). In this many-to-one structure, four different types of input vectors (voltage, current, temperature, and capacity) are associated with single output value (capacity), which also greatly contributes to reducing the number of parameters.

1) MC-LSTM

The input of the proposed model takes the following multi-channel charging profiles of voltage, current, and temperature in addition to capacity as follows:

$$D_k = \begin{cases} V_k^1, V_k^2, \ldots, V_k^S \\ I_k^1, I_k^2, \ldots, I_k^S \\ T_k^1, T_k^2, \ldots, T_k^S \\ C_k \end{cases} \quad (9)$$

$$(D_{k+1}, \ldots, D_{k+L}) \rightarrow C_{k+L+P} \quad (10)$$

where V_k^s, I_k^s, and T_k^s are the s-th sample point of voltage, current, and temperature at k-th cycle, respectively and S is the number of sample points during one charging profile. The proposed method is called multi-channel LSTM (MC-LSTM) and can take various features that affect the capacity change.

2) SC-LSTM

In order to investigate the advantage of structural change, we also consider the case of $D_k = C_k$ i.e., a simplified version of many-to-one structure without using multi-channel charging profiles. This is called single-channel LSTM (SC-LSTM), and we will see SC-LSTM is also better than the baseline LSTM.

IV. LEARNING PROCESS AND MODEL SELECTION

A. OVERALL FRAMEWORK

In Fig. 5, we overview the proposed framework for predicting battery RUL exploiting multi-channel charging profiles based on LSTM. This framework consists of three steps: data preprocessing, training, and test. In the first step, abnormal data is removed by data cleansing, and we average the data over sampling interval to prevent oscillation in short time interval. Then, we perform min-max normalization and divide the data into training set, validation set and test set. In the second step, the model selection is performed by determining the hyperparameters through cross-validation. In the third step, we use the model determined in the previous step to perform the RUL prediction and progress performance evaluation.

B. DATA PREPROCESSING

To obtain the four capacity degradation curves as shown in Fig. 1, data cleaning is first performed. Before using capacity degradation data for the experiment, abnormal values are replaced by the average of highly correlated data. For efficient learning of LSTM, it is not desired to utilize all data, even

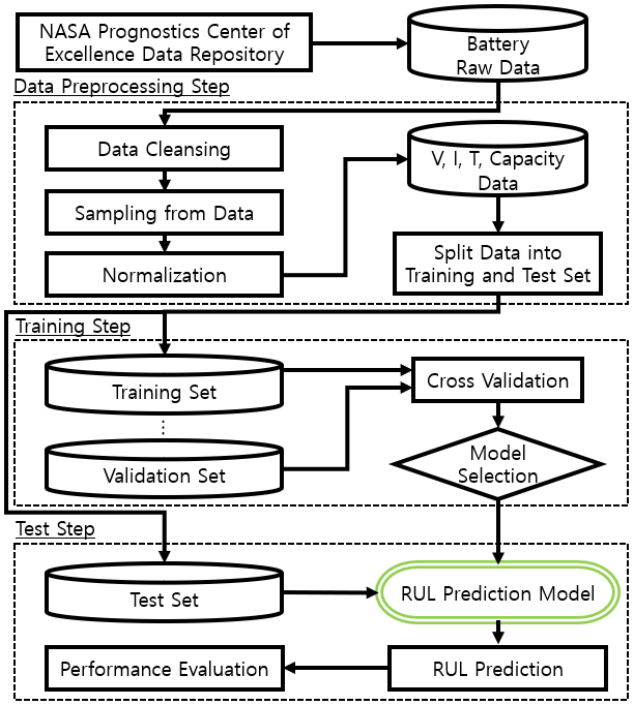

FIGURE 5. An overall framework of the proposed RUL prediction.

if there are many voltage, current and temperature points in the charging process according to the BMS's settings. We choose $S = 10$ in (9), i.e., 10 sample points for each charging profile of voltage, current and temperature as done in [7], [25]. The corresponding input data format is shown in Fig. 6.

After data cleansing, we proceed with data normalization because voltage, current, temperature, and capacity have different scales. In our work, min-max normalization is used as follows [26]:

$$z_k^s = \frac{x_k^s - \min(\mathbf{x})}{\max(\mathbf{x}) - \min(\mathbf{x})} \quad s \in \{1, \ldots, S\} \tag{11}$$

where $\mathbf{x}$ is a collection of all charging cycles $\{x_k^s\}$. The values of voltage, current, and temperature in (10) are the ones after min-max normalization. When presenting the final estimated capacity results, denormalization is performed.

C. MODEL SELECTION

Since acquiring battery charging and discharging data is an expensive process both in terms of time and cost, the NASA datasets of battery charging and discharging are commonly used as a common reference [7], [27]–[29]. Since the available data is limited, we use cross-validation to determine hyperparameters. Specifically, for example, when the battery #5 is used for a test set, two battery sets out of batteries #6, #7, and #18 are used for training set, and the remaining one is used for validation set. This process is repeated three times for each validation set, i.e., we apply 3-fold cross-validation. The detailed process is illustrated in Fig. 6. The hyperparameters are the learning rate, the number of iterations, the number of LSTM cells, and the size of hidden nodes. For the performance metric, we mainly use the mean absolute percentage error (MAPE) while the root mean square error (RMSE) and the mean absolute error (MAE) are

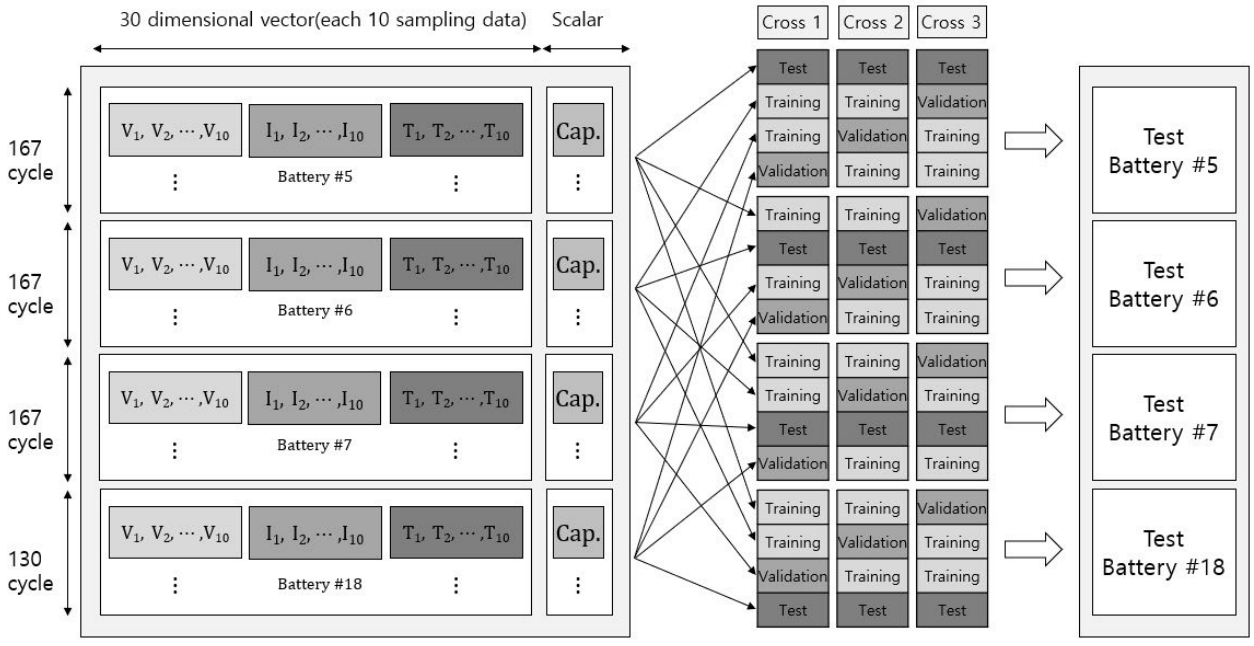

FIGURE 6. Input format and configurations for training, validation and testing.

TABLE 2. Cross-validation error (MAPE) in determining the number of LSTM cells.

Number of LSTM cells	Battery #5	Battery #6	Battery #7	Battery #18
5	2.77	1.47	2.69	7.33
10	2.77	0.70	2.13	2.21
15	2.94	1.13	2.86	2.25
20	2.91	1.23	3.25	2.26
25	17.07	1.49	3.46	7.92
30	16.84	1.20	2.53	3.05

TABLE 3. Cross-validation error (MAPE) in determining the number of hidden nodes.

Number of hidden nodes	Battery #5	Battery #6	Battery #7	Battery #18
10	1.05	0.92	0.56	2.02
20	2.27	0.99	1.39	2.50
30	1.55	1.00	1.16	6.56
40	2.61	0.92	1.29	5.25
50	1.54	0.71	1.56	3.71
60	1.06	0.70	1.79	4.81

also considered:

$$MAPE(\%) = \frac{100}{K}\sum_{k=1}^{K}\frac{\left|C_k - \hat{C}_k\right|}{C_k}, \tag{12}$$

$$RMSE = \sqrt{\frac{1}{K}\sum_{k=1}^{K}(C_k - \hat{C}_k)^2}, \tag{13}$$

$$MAE = \frac{1}{K}\sum_{k=1}^{K}\left|C_k - \hat{C}_k\right| \tag{14}$$

where C_k is the ground-truth capacity, $\hat{C}_k$ is the estimated capacity, and K is the number of cycles.

Now we determine the learning model. All frameworks are built by Tensorflow in Python [30] with the Intel i7-7700 CPU of 3.60 GHz and 16 GB memory, and the average training time is less than 20 seconds. The iterations are set to 500 using early stopping [31]. The model is optimized using the Adam-optimizer with a recommended learning rate of 0.001 [32]. For an activation function, ReLU [33] is adopted. The selection process of sequence length (the number of LSTM cells) is shown in Table 2. The number of hidden nodes specifies the vector size of the LSTM internal values, and shown in Table 3. We determine the hyperparameters for each test battery separately, and in the Table 2 and Table 3 we show them in 5 or 10 units, but in the experiment, we compare MAPE every 1 unit. As a result, our final learning model is such that the number of LSTM cells is 10, the number of hidden nodes is 9 for battery #5, 58 for battery #6, 13 for battery #7, and 4 for battery #18. The final model is shown in Table 4.

V. EXPERIMENT RESULTS

In this section, we provide the experimental results for the cases of battery test sets #5, #6, #7, and #18, respectively. Among various neural network techniques, we use the LSTM in [1], [15], [19], [20] as our baseline since LSTM is known to outperform other methods such as deep neural network (DNN) or convolutional neural network (CNN) for battery capacity estimation [7].

TABLE 4. Selected structure.

Hyperparameters	Baseline LSTM	Proposed LSTM	
	Single-channel	Single-channel	Multi-channel
Learning rate	0.001	0.001	0.001
Number of iterations	500	500	500
Number of LSTM cells	10	10	10
Prediction interval	30	30	30
Size of hidden nodes	60.75	12.5	21

A. CAPACITY REGENERATION AND RUL PREDICTION

1) MODERATE CAPACITY REGENERATION

We first consider the case when the capacity regeneration is moderate, which is observed in battery #5. In this case, the baseline LSTM is slightly better than the proposed one; the MAPE of the baseline is 0.6% while MC-LSTM achieves 1.05% as summarized in Table 5. As can be seen in Fig. 7(a), battery #5 has a rather regular capacity degradation pattern without showing noticeable capacity regeneration, and thus, the baseline LSTM using one-to-one structure works well. However, capacity regeneration occurs typically in lithium-ion batteries [1], [7], [15] as we will see in the cases of batteries #6, #7, and #18.

2) CONSPICUOUS CAPACITY REGENERATION

Noticeable capacity regeneration is observed in batteries #6, #7 and #18. To accurately capture this regeneration phenomenon, we apply two techniques as proposed in Section III-B: many-to-one input/output structure and multi-channel charging profiles. Since RUL prediction is important at every cycle, many-to-one structure is preferred rather than the commonly used many-to-many or one-to-one (baseline) [19], [20]; many-to-many or one-to-one structure shows excellent performance in time-series forecasting, but training in such a way cannot capture the exact regeneration pattern. To demonstrate this, we first show the result of many-to-one structure but without using multi-channel charging profiles, i.e., SC-LSTM. In overall, the proposed SC-LSTM has 39.2% of MAPE improvement compared to the baseline LSTM. Specifically, as shown in Table 5, the MAPEs are reduced from 2.38% to 0.75% (battery #6), from 1.80% to 1.53% (battery #7), and from 6.45% to 3.09% (battery #18), respectively. MAPE is more noticeably reduced when capacity regeneration is conspicuous, see Figs. 7 (b) and (d), which shows the significance of many-to-one structure in using LSTM for RUL prediction.

TABLE 5. RUL prediction result.

Model	Battery #5			Battery #6			Battery #7			Battery #18		
	RMSE	MAE	MAPE	RMSE	MAE	MAPE	RMSE	MAE	MAPE	RMSE	MAE	MAPE
Baseline LSTM	0.0121	0.0085	0.60	0.0468	0.0349	2.38	0.0297	0.0257	1.80	0.0949	0.0899	6.45
SC-LSTM	0.0245	0.0203	1.46	0.0181	0.0110	0.75	0.0271	0.0219	1.53	0.0452	0.0430	3.09
MC-LSTM	0.0168	0.0146	1.05	0.0152	0.0103	0.70	0.0085	0.0068	0.47	0.0388	0.0261	1.88

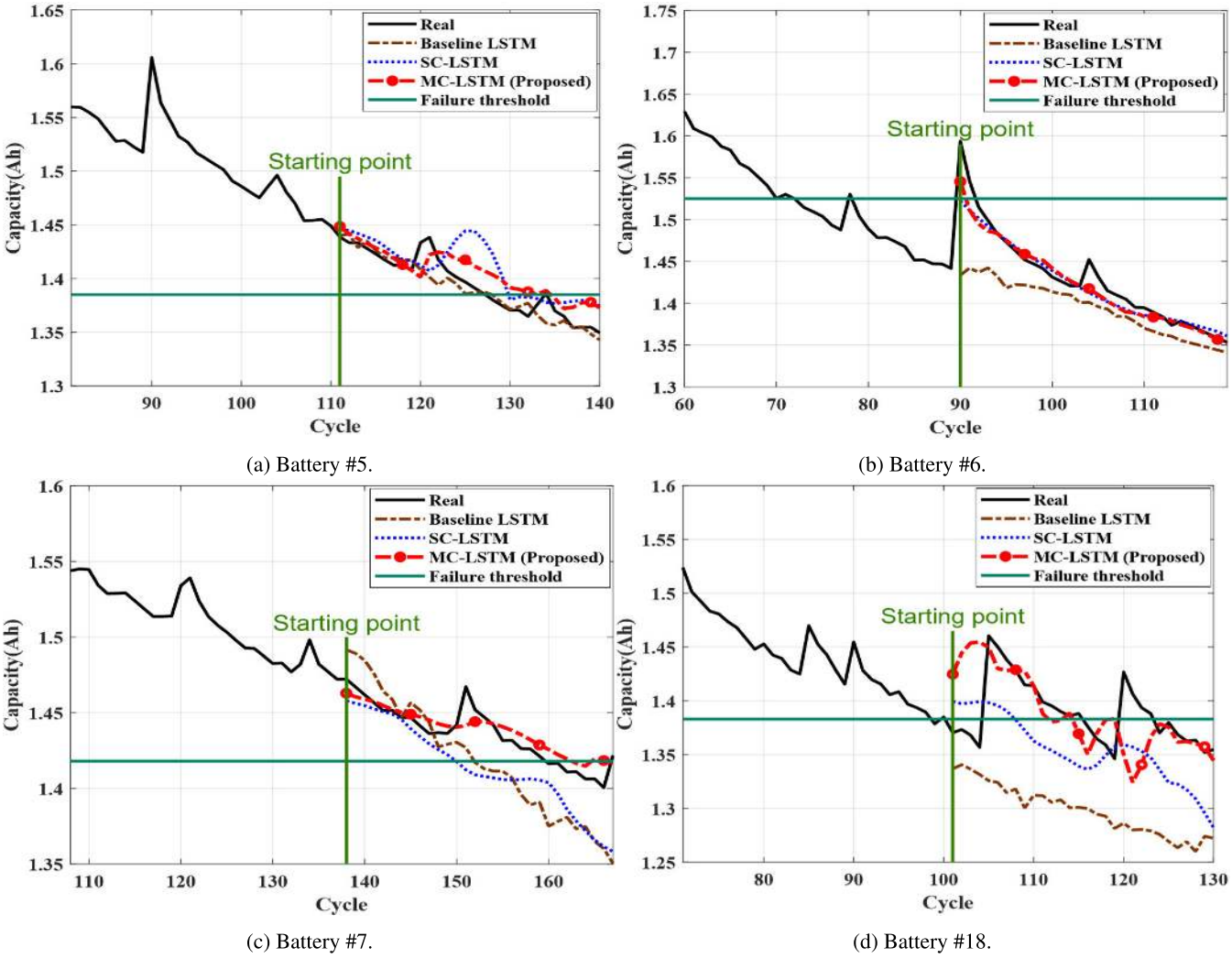

(a) Battery #5.

(b) Battery #6.

(c) Battery #7.

(d) Battery #18.

FIGURE 7. RUL prediction result.

Performance improvement is further significant when multi-channel charging profiles of voltage, current and temperature are collectively incorporated. In overall, the proposed MC-LSTM outperforms the baseline LSTM; the performance has been enhanced by up to 63.7% in terms of MAPE. Specifically, the MAPE of the proposed MC-LSTM is 0.70% for battery #6, 0.47% for battery #7, and 1.88% for battery #18, which are substantially lower than those of the baseline. Interestingly, capacity regeneration immediately occurs at the first RUL prediction cycle in the case of battery #6, see Fig. 7(b). Nevertheless, MC-LSTM closely follows the true values while the baseline does not catch them at all. In the case of battery #18, RUL prediction is challenging because the capacity degradation pattern is different from others, see Fig. 1. Nevertheless, the proposed methods show much smaller MAPEs than that of the baseline.

B. COMPARISON WITH VARIOUS RNN MODELS WITH MULTI-CHANNEL CHARGING PROFILES

One might wonder if other RNN based models would perform better for RUL prediction. To investigate this, we further compare the proposed LSTM method with basic RNN, GRU, and

TABLE 6. Comparison with various RNN based models with multi-channel charging profiles.

Model	Battery #5			Battery #6			Battery #7			Battery #18		
	RMSE	MAE	MAPE	RMSE	MAE	MAPE	RMSE	MAE	MAPE	RMSE	MAE	MAPE
MC-RNN	0.0302	0.0284	2.05	0.0339	0.0272	1.86	0.0204	0.0184	1.27	0.0369	0.0304	2.19
MC-GRU	0.0213	0.0195	1.41	0.0271	0.0180	1.21	0.0200	0.0186	1.29	0.0433	0.0294	2.14
MC-SRU	0.0202	0.0171	1.22	0.0504	0.0478	3.34	0.0163	0.0126	0.88	0.0585	0.0427	3.09
MC-LSTM	0.0168	0.0146	1.05	0.0152	0.0103	0.70	0.0085	0.0068	0.47	0.0388	0.0261	1.88

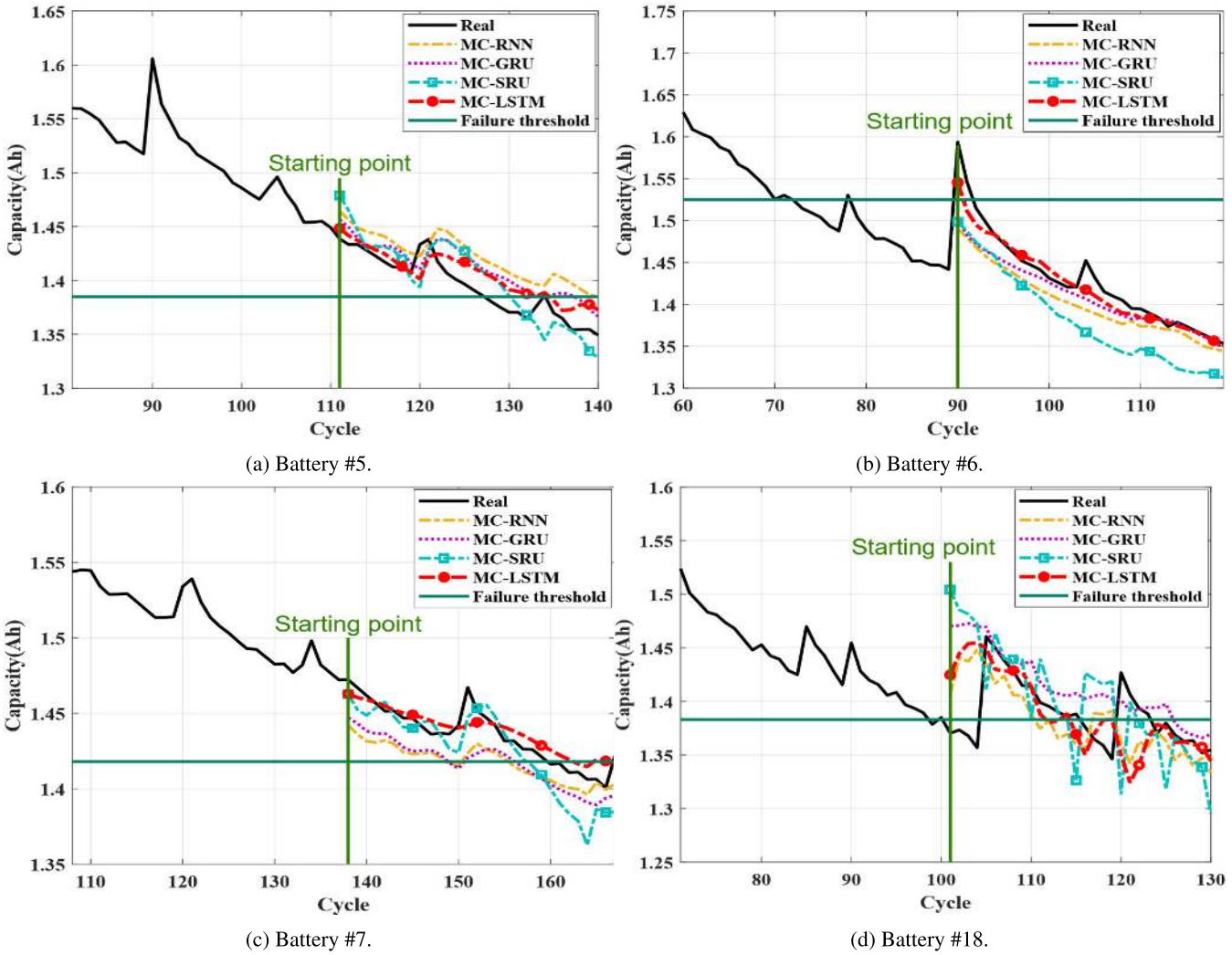

(a) Battery #5.

(b) Battery #6.

(c) Battery #7.

(d) Battery #18.

FIGURE 8. Comparison with various RNN based models with multi-channel charging profiles.

SRU, all of which also use multi-channel charging profiles. The structures of RNN, GRU, and SRU are determined by cross-validation as we did in Section IV-C. The selected structure and hyperparameters are the same as the case of LSTM except for the number of hidden nodes, which are 25.25, 33.75, 34.25 for RNN, GRU, and SRU, respectively. Since many-to-one structure shows better RUL prediction, we apply that to all models. The result is summarized in Table 6. As can be seen, MC-LSTM outperforms all MC-RNN, MC-GRU, and MC-SRU; for example, in the case of MAPE, MC-LSTM is better than the best of three by 32–52%. The average MAPEs for all batteries are summarized in Table 7; the results are 1.84%, 1.51% and 2.13%, and 1.02% for MC-RNN, MC-GRU, MC-SRU, and MC-LSTM, respectively. Since RNN has the simplest structure out of four, the highest error performance is not unusual. In the case of GRU, the reason for high error comes from that GRU has only two gates while LSTM has three. The internal memory cell of GRU is not different from the hidden state value seen from the outside, so the LSTM is more powerful and flexible. In the

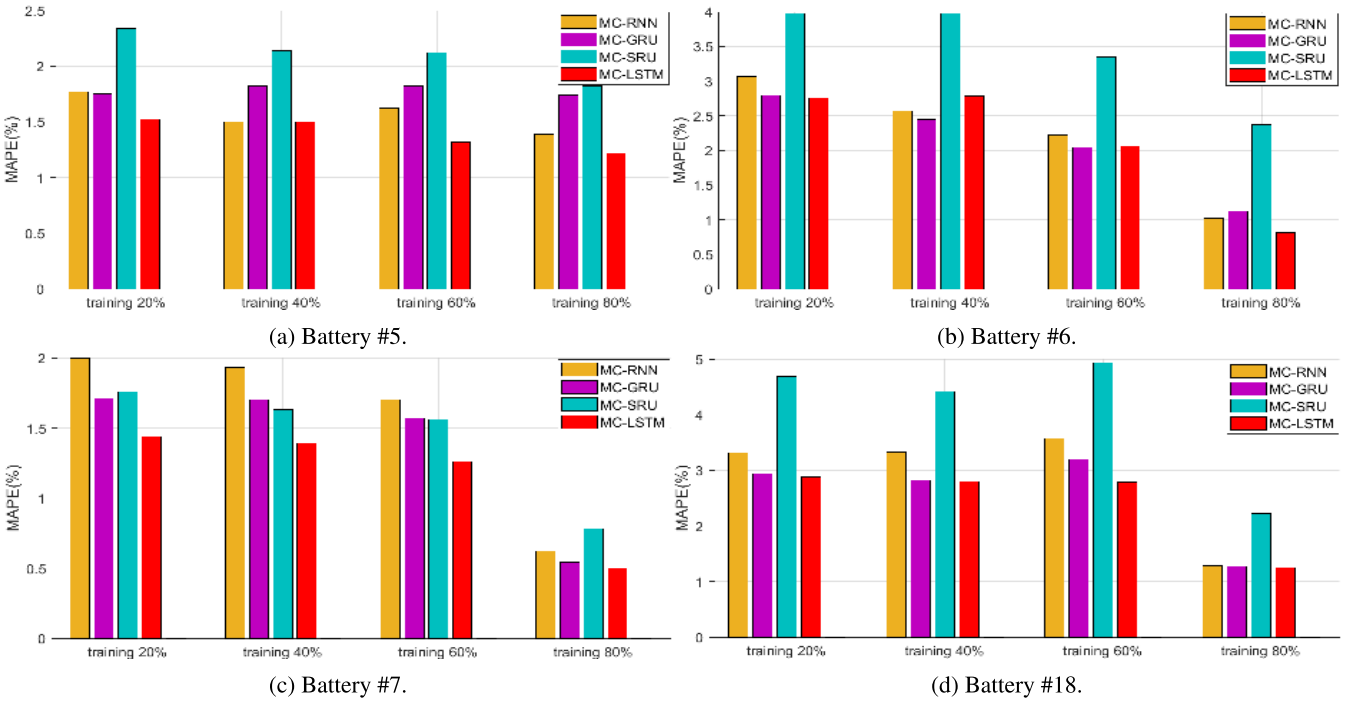

(a) Battery #5.

(b) Battery #6.

(c) Battery #7.

(d) Battery #18.

FIGURE 9. Comparison with various training set ratios.

TABLE 7. Model complexity and MAPE comparison.

Model	Parameters	MAPE(%)
Baseline LSTM	22,295	2.81
SC-LSTM	725	1.71
MC-RNN	1,446	1.84
MC-GRU	6,657	1.51
MC-SRU	3,185	2.13
MC-LSTM	2,772	1.02

case of SRU, most of RNN's operations are independent of recurrence, which is good for fast computation. However, it results in poor accuracy in the presence of capacity regeneration. Fig. 8 shows the RUL prediction of four methods, and MC-LSTM more closely follows the real data than other three methods.

C. MODEL COMPLEXITY AND RUL PREDICTION

Table 7 also shows the number of parameters (i.e., the model complexity) and RUL prediction accuracy; LSTM has an iterative structure in time, and the number of parameters is affected by the size of input data and the size of hidden nodes. Since the proposed LSTM uses many-to-one structure, the number of required hidden nodes is much smaller than one-to-one structure of the baseline LSTM. This significantly reduces the number of parameters, e.g., by 8 to 30 times smaller than that of the baseline, and this is also beneficial for better generalization. In the case of MC-RNN, MC-GRU and MC-SRU, the number of hidden nodes is determined by cross-validation, and it results in the increased number of parameters as can be seen in Table 7.

D. PREDICTION ACCURACY WITH VARIOUS STARTING POINTS

As the starting point of RUL prediction shifts to early cycles, the models can leverage fewer data (i.e., small training set), which makes RUL prediction harder. To investigate the impact of varying the size of training set, we perform experiment by setting the size of training set as 80%, 60%, 40% and (around) 20% of the whole cycles. As we discussed in Section IV-C and Fig. 6, for one test battery set, three other battery sets are used for training and validation sets. Since the number of available cycles is different for four batteries, the smallest size of training set is either 24% or 30%, depending on the types of test batteries. The earliest starting point is 40th cycle because the number of LSTM cells is 10 and the prediction interval is 30. The corresponding results are shown in Fig. 9, Table 8, Table 9, Table 10, and Table 11.

E. ESTIMATING THE END OF LIFE

Finally, we estimate the end of life (EoL), i.e., when battery capacity reaches the failure threshold; this is the main purpose of RUL prediction. We compare the estimation accuracy of EoL, and the result is summarized in terms of mean, standard deviation, and 95% confidence bound in Table 12. It should be noted that, due to capacity regeneration, EoL need to be defined as the last moment to hit the EoL threshold, rather than the first moment. Recall that we set the EoL when SoH reaches 75.2%. As can be seen in Table 12, the base-

TABLE 8. Comparison with various starting points (Battery #5).

Model	training 80%, predict 20%			training 60%, predict 40%			training 40%, predict 60%			training 24%, predict 76%		
	RMSE	MAE	MAPE	RMSE	MAE	MAPE	RMSE	MAE	MAPE	RMSE	MAE	MAPE
MC-RNN	0.0200	0.0184	1.39	0.0255	0.0223	1.62	0.0276	0.0219	1.50	0.0343	0.0272	1.77
MC-GRU	0.0262	0.0231	1.74	0.0282	0.0250	1.82	0.0286	0.0258	1.82	0.0299	0.0254	1.75
MC-SRU	0.0284	0.0233	1.82	0.0322	0.0291	2.12	0.0356	0.0303	2.14	0.0440	0.0340	2.34
MC-LSTM	0.0205	0.0164	1.22	0.0208	0.0181	1.32	0.0250	0.0215	1.50	0.0269	0.0223	1.52

TABLE 9. Comparison with various starting points (Battery #6).

Model	training 80%, predict 20%			training 60%, predict 40%			training 40%, predict 60%			training 30%, predict 70%		
	RMSE	MAE	MAPE	RMSE	MAE	MAPE	RMSE	MAE	MAPE	RMSE	MAE	MAPE
MC-RNN	0.0172	0.0141	1.02	0.0488	0.0323	2.22	0.0448	0.0381	2.57	0.0540	0.0469	3.07
MC-GRU	0.0218	0.0155	1.12	0.0375	0.0296	2.04	0.0481	0.0370	2.45	0.0524	0.0429	2.79
MC-SRU	0.0385	0.0329	2.37	0.0624	0.0485	3.35	0.0647	0.0591	3.98	0.0698	0.0604	3.98
MC-LSTM	0.0170	0.0111	0.81	0.0428	0.0299	2.06	0.0524	0.0431	2.78	0.0511	0.0423	2.76

TABLE 10. Comparison with various starting points (Battery #7).

Model	training 80%, predict 20%			training 60%, predict 40%			training 40%, predict 60%			training 24%, predict 76%		
	RMSE	MAE	MAPE	RMSE	MAE	MAPE	RMSE	MAE	MAPE	RMSE	MAE	MAPE
MC-RNN	0.0119	0.0089	0.62	0.0284	0.0255	1.70	0.0322	0.0292	1.93	0.0383	0.0318	2.00
MC-GRU	0.0099	0.0078	0.54	0.0269	0.0234	1.57	0.0298	0.0260	1.70	0.0333	0.0271	1.71
MC-SRU	0.0140	0.0198	0.78	0.0296	0.0241	1.56	0.0311	0.0249	1.63	0.0386	0.0283	1.76
MC-LSTM	0.0088	0.0072	0.50	0.0231	0.0190	1.26	0.0281	0.0214	1.39	0.0264	0.0224	1.44

TABLE 11. Comparison with various starting points (Battery #18).

Model	training 80%, predict 20%			training 60%, predict 40%			training 40%, predict 60%			training 30%, predict 70%		
	RMSE	MAE	MAPE	RMSE	MAE	MAPE	RMSE	MAE	MAPE	RMSE	MAE	MAPE
MC-RNN	0.0231	0.0177	1.28	0.0645	0.0504	3.57	0.0600	0.0479	3.33	0.0619	0.0485	3.31
MC-GRU	0.0228	0.0176	1.27	0.0568	0.0453	3.20	0.0539	0.0408	2.82	0.0517	0.0433	2.94
MC-SRU	0.0419	0.0309	2.23	0.0800	0.0698	4.94	0.0756	0.0636	4.42	0.0831	0.0685	4.69
MC-LSTM	0.0209	0.0173	1.25	0.0449	0.0393	2.79	0.0503	0.0403	2.80	0.0532	0.0424	2.88

TABLE 12. End of life (EoL) accuracy in terms of mean, standard deviation (STD) and confidence bound (CB).

Model	Battery #5 (EoL = 134)			Battery #6 (EoL = 92)			Battery #7 (EoL = 167)			Battery #18 (EoL = 124)		
	Mean	STD	95% CB	Mean	STD	95% CB	Mean	STD	95% CB	Mean	STD	95% CB
Baseline LSTM	127.9	0.99	[127, 130]	75.2	1.69	[72, 78]	150.8	1.60	[147, 153]	98.8	2.15	[95, 101]
SC-LSTM	130.8	2.31	[128, 135]	90.2	0.79	[89, 91]	150.1	2.53	[143, 153]	108.7	0.82	[108, 110]
MC-RNN	136.5	6.05	[128, 140]	87.6	0.49	[87, 88]	152.6	6.74	[145, 161]	118.9	7.34	[108, 127]
MC-GRU	140.4	2.06	[138, 144]	88	2.28	[84, 90]	157.9	0.94	[157, 160]	127.9	1.92	[126, 130]
MC-SRU	128.6	3.14	[123, 132]	88.6	0.49	[88, 89]	150.9	9.20	[138, 159]	115.8	6.08	[108, 122]
MC-LSTM	131.4	2.56	[129, 135]	90.6	0.52	[90, 91]	159.6	5.46	[153, 167]	119.1	6.67	[109, 125]

line estimates the EoL too early. For example, in the case of battery #6, the true EoL is at 92th cycle, but the baseline's estimation is at 75th cycle. In the case of battery #18, the true EoL is at 124th cycle, but the baseline's estimation is at 98th cycle. Considering that lithium-ion batteries are expensive, precocious estimation of EoL results in wasting usable batteries. By contrast, MC-LSTM estimates the EoL of batteries accurately, and also *before* the true EoL, which is important for safe operation; for example, in the case of batteries #6 and #18, MC-LSTM's estimation is at 90th cycle and at 119th cycle, respectively, which are only a few cycles ahead of the true values. This demonstrates that accurate EoL estimation is possible under the presence of capacity regeneration. In the case of MC-RNN, MC-GRU and MC-SRU, the end of life prediction is better than the baseline LSTM or SC-LSTM, but in overall, MC-LSTM predicts the most accurately, i.e., the closest to the true EoL while not exceeding that.

VI. CONCLUSION

In this paper, we proposed data-driven LSTM-based RUL prediction methods for lithium-ion batteries. We proposed to use the many-to-one structure instead of the one-to-one structure to accurately predict RUL. We demonstrated that this structure change is effective to capture the capacity regeneration phenomenon. In addition, the many-to-one structure significantly reduces the number of parameters, which is desired for better generalization. We then exploited the multi-channel charging profiles of voltage, current, and temperature, which are the essential features for RUL prediction. Experiments on NASA lithium-ion battery datasets verified that the proposed methods predict RUL accurately. The proposed MC-LSTM improves the MAPE by 63.7% compared to the baseline and achieves 0.47%–1.88% of MAPE in overall. Furthermore, MC-LSTM is significantly better than the baseline in estimating the EoL, which leads to utilizing batteries without prematurely declaring the end of use.

REFERENCES

[1] R. Xiong, Y. Zhang, J. Wang, H. He, S. Peng, and M. Pecht, "Lithium-ion battery health prognosis based on a real battery management system used in electric vehicles," *IEEE Trans. Veh. Technol.*, vol. 68, no. 5, pp. 4110–4121, May 2019.

[2] J. Meng, D.-I. Stroe, M. Ricco, G. Luo, and R. Teodorescu, "A simplified model-based state-of-charge estimation approach for lithium-ion battery with dynamic linear model," *IEEE Trans. Ind. Electron.*, vol. 66, no. 10, pp. 7717–7727, Oct. 2019.

[3] J. Zhang and J. Lee, "A review on prognostics and health monitoring of Li-ion battery," *J. Power Sources*, vol. 196, no. 15, pp. 6007–6014, Aug. 2011.

[4] S. Voronov, E. Frisk, and M. Krysander, "Data-driven battery lifetime prediction and confidence estimation for heavy-duty trucks," *IEEE Trans. Rel.*, vol. 67, no. 2, pp. 623–639, Jun. 2018.

[5] J. Qu, F. Liu, Y. Ma, and J. Fan, "A neural-network-based method for RUL prediction and SOH monitoring of lithium-ion battery," *IEEE Access*, vol. 7, pp. 87178–87191, 2019.

[6] X. Wang, C. Hu, X. Si, Z. Pang, and Z. Ren, "An adaptive remaining useful life estimation approach for newly developed system based on nonlinear degradation model," *IEEE Access*, vol. 7, pp. 82162–82173, 2019.

[7] Y. Choi, S. Ryu, K. Park, and H. Kim, "Machine learning-based lithium-ion battery capacity estimation exploiting multi-channel charging profiles," *IEEE Access*, vol. 7, pp. 75143–75152, 2019.

[8] T. Biagetti, "Automatic diagnostics and prognostics of energy conversion processes via knowledge-based systems," *Energy*, vol. 29, nos. 12–15, pp. 2553–2572, Dec. 2004.

[9] J. Li, C. Lyu, L. Wang, L. Zhang, and C. Li, "Remaining capacity estimation of Li-ion batteries based on temperature sample entropy and particle filter," *J. Power Sources*, vol. 268, pp. 895–903, Dec. 2014.

[10] A. Nuhic, T. Terzimehic, T. Soczka-Guth, M. Buchholz, and K. Dietmayer, "Health diagnosis and remaining useful life prognostics of lithium-ion batteries using data-driven methods," *J. Power Source*, vol. 239, pp. 680–688, Oct. 2013.

[11] D. Liu, J. Zhou, H. Liao, Y. Peng, and X. Peng, "A health indicator extraction and optimization framework for lithium-ion battery degradation modeling and prognostics," *IEEE Trans. Syst., Man, Cybern., Syst.*, vol. 45, no. 6, pp. 915–928, Jun. 2015.

[12] M. A. Patil, P. Tagade, K. S. Hariharan, S. M. Kolake, T. Song, T. Yeo, and S. Doo, "A novel multistage support vector machine based approach for Li ion battery remaining useful life estimation," *Appl. Energy*, vol. 159, pp. 285–297, Dec. 2015.

[13] J. Liu, A. Saxena, K. Goebel, B. Saha, and W. Wang, "An adaptive recurrent neural network for remaining useful life prediction of lithium-ion batteries," *Proc. Annu. Conf. Prognostics Health Manage. Soc.*, 2010, pp. 1–9.

[14] Y. Zhang, R. Xiong, H. He, and M. G. Pecht, "Long short-term memory recurrent neural network for remaining useful life prediction of lithium-ion batteries," *IEEE Trans. Veh. Technol.*, vol. 67, no. 7, pp. 5695–5705, Jul. 2018.

[15] X. Li, L. Zhang, Z. Wang, and P. Dong, "Remaining useful life prediction for lithium-ion batteries based on a hybrid model combining the long short-term memory and Elman neural networks," *J. Energy Storage*, vol. 21, pp. 510–518, Feb. 2019.

[16] Y. Bengio, P. Simard, and P. Frasconi, "Learning long-term dependencies with gradient descent is difficult," *IEEE Trans. Neural Netw.*, vol. 5, no. 2, pp. 157–166, Mar. 1994.

[17] B. Xiao, Y. Liu, and B. Xiao, "Accurate state-of-charge estimation approach for lithium-ion batteries by gated recurrent unit with ensemble optimizer," *IEEE Access*, vol. 7, pp. 54192–54202, 2019.

[18] Y. Song, L. Li, Y. Peng, and D. Liu, "Lithium-ion battery remaining useful life prediction based on GRU-RNN," in *Proc. 12th Int. Conf. Rel., Maintainability, Saf. (ICRMS)*, Oct. 2018, pp. 317–322.

[19] F. Zhou, P. Hu, and X. Yang, "RUL prognostics method based on real time updating of LSTM parameters," in *Proc. Chin. Control Decis. Conf. (CCDC)*, Jun. 2018, pp. 3966–3971.

[20] Y. Liu, G. Zhao, X. peng, and C. Hu, "Lithium-ion battery remaining useful life prediction with long short-term memory recurrent neural network," in *Proc. Annu. Conf. Prognostics Health Manage. Soc.*, Oct. 2017, no. 1, pp. 1–7.

[21] T. Lei, Y. Zhang, S. I. Wang, H. Dai, and Y. Artzi, "Simple recurrent units for highly parallelizable recurrence," in *Proc. Conf. Empirical Methods Natural Lang. Process.*, 2018, pp. 4470–4481.

[22] B. Saha and K. Goebel. (2007). Battery Data Set. NASA Ames Prognostics Data Repository, Moffett Field, CA, USA. Accessed: Sep. 1, 2018. [Online]. Available: http://ti.arc.nasa.gov/project/prognostic-data-repository and https://ti.arc.nasa.gov/tech/dash/groups/pcoe/prognostic-data-repository/

[23] Y. Zhou, M. Huang, and M. Pecht, "Remaining useful life estimation of lithium-ion cells based on k-nearest neighbor regression with differential evolution optimization," *J. Cleaner Prod.*, vol. 249, Mar. 2020, Art. no. 119409.

[24] X. Hu, J. Jiang, D. Cao, and B. Egardt, "Battery health prognosis for electric vehicles using sample entropy and sparse Bayesian predictive modeling," *IEEE Trans. Ind. Electron.*, vol. 63, no. 4, pp. 2645–2656, Apr. 2016.

[25] J. Wu, C. Zhang, and Z. Chen, "An online method for lithium-ion battery remaining useful life estimation using importance sampling and neural networks," *Appl. Energy*, vol. 173, pp. 134–140, Jul. 2016.

[26] A. Jain, K. Nandakumar, and A. Ross, "Score normalization in multimodal biometric systems," *Pattern Recognit.*, vol. 38, no. 12, pp. 2270–2285, Dec. 2005.

[27] L. Ren, L. Zhao, S. Hong, S. Zhao, H. Wang, and L. Zhang, "Remaining useful life prediction for lithium-ion battery: A deep learning approach," *IEEE Access*, vol. 6, pp. 50587–50598, 2018.

[28] Z. Wu, Z. Wang, C. Qian, B. Sun, Y. Ren, Q. Feng, and D. Yang, "Online prognostication of remaining useful life for random discharge lithium-ion batteries using a gamma process model," in *Proc. 20th Int. Conf. Therm., Mech. Multi-Phys. Simulation Exp. Microelectron. Microsyst. (EuroSimE)*, Mar. 2019, pp. 1–6.

[29] Z. Zheng, J. Peng, K. Deng, K. Gao, H. Li, B. Chen, Y. Yang, and Z. Huang, "A novel method for lithium-ion battery remaining useful life prediction using time window and gradient boosting decision trees," in *Proc. 10th Int. Conf. Power Electron. ECCE Asia*, May 2019, pp. 3297–3302.

[30] M. Abadi *et al.*, "Tensorflow: A system for large-scale machine learning," in *Proc. OSDI*, vol. 16, 2016, pp. 265–283.

[31] L. Prechelt, "Early stopping-but when?" *Neural Networks: Tricks of the Trade*. Berlin, Germany: Springer, 2012, pp. 53–67.

[32] D. P. Kingma and J. Ba, "Adam: A method for stochastic optimization," in *Proc. Int. Conf. Learn. Represent.*, May 2015, pp. 1–13.

[33] V. Nair and G. E. Hinton, "Rectified linear units improve restricted Boltzmann machines," in *Proc. Int. Conf. Mach. Learn.*, 2010, pp. 807–814.

KYUNGNAM PARK received the B.S. and M.S. degrees in electronic engineering from Sogang University, in 2019 and 2017, respectively. His research interests are energy analytics, recurrent neural networks, load forecasting, and generative adversarial networks. He was a recipient of full scholarship for excellent undergraduate GPA, in 2017, and CSAT math and science scores, in 2012, in the Department of Electronic Engineering, Sogang University, respectively.

YOHWAN CHOI received the B.S. and Ph.D. degrees in electronic engineering from Sogang University, in 2013 and 2019, respectively. His research interests are state of health estimation, smart battery management, energy storage systems, and power economics and optimization.

WON JAE CHOI received the B.S. and Ph.D. degrees in chemical biotechnology from Seoul National University. He is currently a Senior Research Engineer of the Energy Storage System Development Team, Hyundai Motor Company, South Korea.

HEE-YEON RYU received the Ph.D. degree in mechanical engineering from the University of Colorado at Boulder. He is currently a Team Leader of the Energy Storage System Development Team, Hyundai Motor Company, South Korea.

HONGSEOK KIM (Senior Member, IEEE) received the B.S. and M.S. degrees in electrical engineering from Seoul National University, in 1998 and 2000, respectively, and the Ph.D. degree in electrical and computer engineering from The University of Texas at Austin, in 2009. He was a member of Technical Staff with Korea Telecom Labs, from 2000 to 2005. He was a Postdoctoral Research Associate with the Department of Electrical Engineering, Princeton University, from 2009 to 2010. He was a member of Technical Staff with Bell Labs, USA, from 2010 to 2011. He is currently an Associate Professor with the Department of Electronic Engineering, Sogang University, South Korea. His research interests include smart grid and energy ICT, specifically focused on machine learning for energy forecasting, energy trading and electricity market, energy storage systems, microgrid, optimal power flow, and wireless networks. He was a recipient of the Korea Government Overseas Scholarship, from 2005 to 2008. He received the Haedong Young Professional Award, in 2016. He served as an Editor for *Journal of Communications and Networks* and the Guest Editor for Energies with the special issue of Machine Learning and Optimization with Applications of Power System.